International Journal of Thermophysics, Vol. 15, No. 2, 1994

A High-Temperature Laser-Pulse Thermal Diffusivity Apparatus

A. Cezairliyan,[1] T. Baba,[1,2] and R. Taylor[1,3]

Received September 15, 1993

A high-temperature laser-pulse apparatus for the measurement of thermal diffusivity in the temperature range from 1500 to 2500 K has been designed, constructed, and tested at the National Institute of Standards and Technology. A curve-fitting method is introduced by which the entire experimental temperature history curve is fitted with the theoretical curve under the boundary condition of radiative heat losses. The new apparatus and the curve-fitting method permit thermal diffusivity measurements with an uncertainty of not more than 3%.

KEY WORDS: high temperature; laser pulse method; thermal diffusivity.

1. INTRODUCTION

The pulse method for measuring thermal diffusivity was developed by Parker et al. [1] in 1961. Now the laser-pulse method is generally recognized as the preferred method for measuring the thermal diffusivity of solid materials from room temperature to high temperatures [2]. Since accurate measurement of thermal conductivity by steady-state methods is difficult above about 1500 K, it is common practice to determine thermal conductivity from measurements of thermal diffusivity, assuming that specific heat and density data are available [3].

Laser-pulse thermal diffusivity measurements performed above 1500 K are considerably more difficult than those made at lower temperatures for

[1] Metallurgy Division, National Institute of Standards and Technology, Gaithersburg, Maryland 20899, U.S.A..

[2] Guest Scientist from the Thermophysical Metrology Department, National Research Laboratory of Metrology, Tsukuba, Ibaraki 305, Japan.

[3] Guest Scientist from the Material Science Centre, University of Manchester/UMIST, Manchester, M1 7HS, United Kingdom.

0195-928X/94/0300-0317$07.00/0

840/15/2-9

several reasons. The specimen cannot be held under adiabatic conditions because of radiative heat loss from its surfaces. Also, several experimental problems must be solved, which include overheating of the experiment chamber, mechanical vibrations induced by the large alternating electric currents used for the furnace, coating of the optical windows, chemical contamination of the specimen, and changes in the specimen surface. Because of these, there have been only a limited number of laser-pulse thermal diffusivity apparatuses which operated above 2000 K [4–6].

The apparatus described in this paper is designed and constructed primarily for accurate measurements of thermal diffusivity at temperatures from 1500 to 2500 K. A new data processing procedure is introduced which takes radiative heat losses into consideration and determines thermal diffusivity values by fitting the entire experimental curve to Cape and Lehman's theoretical curve [7].

2. MEASUREMENT SYSTEM

Figure 1 shows the functional diagram of the high-temperature laser-pulse thermal diffusivity system developed at the National Institute of Standards and Technology. The system consists of an experiment chamber, a pulsed laser, an automatic pyrometer, a high-speed radiometer, a digital data acquisition system, and a computer. The experiment chamber contains the furnace, the specimen holder, and the specimen and is connected to a vacuum system.

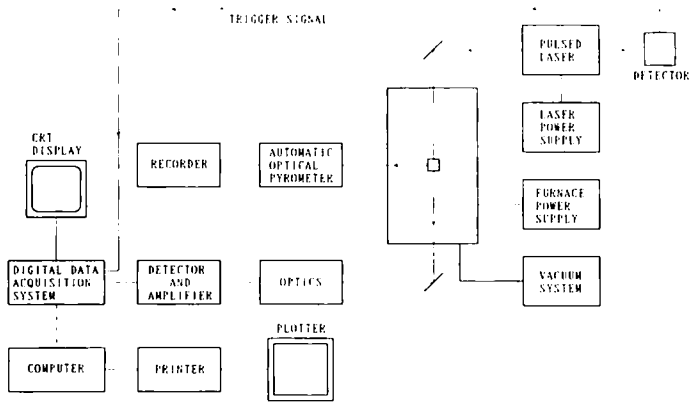

Fig. 1. Functional diagram of the high-temperature laser-pulse thermal diffusivity apparatus.

2.1. Experiment Chamber

Figure 2 shows the internal structure of the high-temperature experiment chamber. The furnace has a vertical cylindrical shape in which the tungsten specimen holder is suspended by three tungsten rods and the tungsten mesh heater surrounds the specimen holder. A high-current AC power supply is used to feed current to the tungsten mesh heater. The experiment chamber is evacuated by a mechanical pump and a diffusion pump to less than 1×10^{-3} Pa at room temperature and to less than 5×10^{-3} Pa at 2500 K.

To reduce radiative heat loss from the heater, the heater is surrounded with several layers of radiation shields. There is a set of seven cylindrical

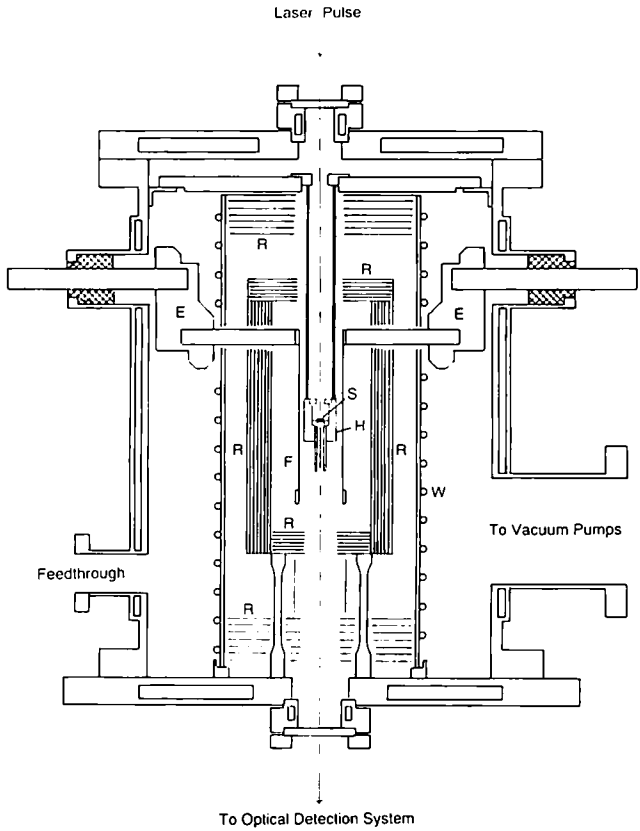

Fig. 2. Internal structure of the high-temperature experiment chamber. E, electrode; F, furnace; H, specimen holder; R, radiation shields; S, specimen; W, water cooling coil

radiation shields in the radial direction, where the inner three layers are tungsten and the outer four layers are molybdenum. There are two sets of planar radiation shields both over and under the heater. The inner set consists of seven tungsten plates for both the top and the bottom parts. The outer set of the top part consists of five molybdenum plates and that of the bottom part consists of seven molybdenum plates. The experiment chamber wall, the top and bottom flanges, the electrodes, and the window frames are all water cooled. An extra copper water jacket is added inside the experiment chamber to improve the cooling of the entire chamber.

The experiment chamber has three optical windows. The one is at the center of the top flange, to permit the pulsed laser beam to impinge on the specimen. The second is at the center of the bottom flange, for optical detection of the transient temperature change of the back surface of the specimen. The third is on the side wall of the experiment chamber, to permit measurement of the steady-state temperature of the specimen by an automatic optical pyrometer.

2.2. Specimen and Specimen Holder

The specimen is in the shape of a small disk (6.3 mm in diameter and 1–3 mm in thickness). The specimen is placed in the tungsten specimen holder as shown in Fig. 3. To reduce heat conduction between the specimen

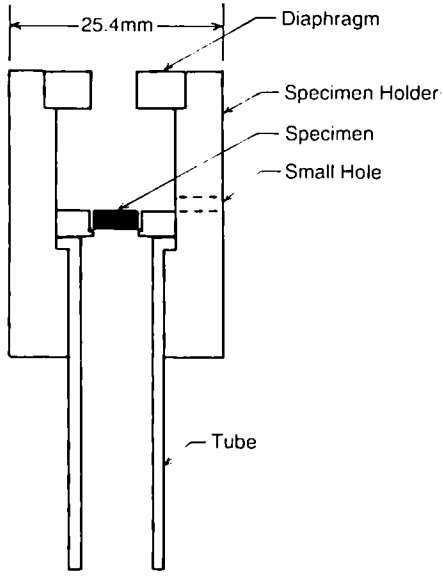

Fig. 3. Tungsten specimen holder.

and the holder, the specimen sits on three tiny projections and is guided by three tiny humps inside the hole. A tungsten diaphragm is placed on the top of the holder. The area of the laser beam is limited by the diameter of the aperture of the diaphragm, which is equal to the diameter of the specimen (6.3 mm).

A tungsten tube is attached to the bottom of the holder to shield the specimen from direct exposure to the heater radiation. Radiation from the back surface of the specimen, used for detecting the temperature change of the specimen, passes through this tube. A small hole (2.4 mm in diameter) in the vertical wall of the specimen holder is used in the measurement of the steady-state temperature of the specimen.

2.3. Automatic Pyrometer

The steady-state temperature of the specimen is measured with a commercial automatic pyrometer. The optics were modified to permit the measurements on a target less than 2 mm in diameter. The temperature resolution is about 0.5 K at 1500 K, increasing to about 1 K at 3000 K. The pyrometer was recalibrated with a NIST calibrated lamp.

2.4. Laser

The neodymium glass laser, used for pulse heating the specimen, has the following specifications.

Wavelength:	1.06 μm.
Glass rod:	270 mm in length and 19 mm in diameter.
Excitation:	single spiral xenon flash lamp.
Pulse duration:	1 ms (nominal).
Oscillation:	multimode.
Energy per pulse:	200 J (max).

In the experiments described here, the laser was operated with an output energy in the range of 40 to 70 J per pulse.

2.5. Detector Optics

The transient temperature of the back surface of the specimen is radiatively detected from outside the experiment chamber through the bottom window. Outside the chamber, radiation from the specimen is reflected by a flat mirror and focused by a telescope onto the end of an optical fiber bundle. The fiber bundle transfers the radiation to a silicon photodiode which is mounted on a box containing the electronics. A band

reject filter reflecting >99.9% at 1.06 μm is interposed in the radiation path, and suitable precautions are taken to screen the detector from stray radiation from the laser and the laser flash tube. The detected area on the specimen is a circle of 2-mm diameter, which is about one-third of the specimen diameter.

2.6. Electronics

The electronics were designed to suppress the steady-state component of the output voltage from the silicon photodiode and amplify only transient components by a factor of 10, 100, or 1000. Batteries are used as the power source for the electronics to eliminate 60-Hz noise. The box containing the electronics is placed about 5 m away from the AC power supply, the experiment chamber, the laser, and the laser power supply to reduce electromagnetically induced noise.

2.7. Digital Data Acquisition System

The electronically amplified signal is recorded with a digital oscilloscope, which has a 4k word memory with 12-bit resolution. Usually, data are recorded every 100 or 200 μs during an experiment. The data stored in the oscilloscope are transferred to a computer for processing.

3. OPERATIONAL CHARACTERISTICS

3.1. Stability of the Steady-State Temperature

Drift in the specimen's steady-state temperature was determined by monitoring the radiation from the back surface of the specimen with the silicon photodiode. A long-term drift was observed even after a nominal equilibrium in the furnace was reached. This drift is attributed to small changes in the output of the AC power supply, which was not feedback controlled. The output of the silicon photodiode was monitored with a storage oscilloscope and the experiments were performed when the specimen temperature was stabilized to within 0.01 $K \cdot s^{-1}$ or better below 2200 K.

Above 2200 K, a short-term drift with an interval of several seconds was superimposed on the long-term drift. The origin of this drift is not known. At 2500 K, the drift grows to about 0.2 $K \cdot s^{-1}$, with an interval of several seconds. Thermal diffusivity measurements are performed when the drift monitored by the storage oscilloscope is small. In this case the drift is expected to be less than 0.05 $K \cdot s^{-1}$ during the experiment. This short-

term temperature drift limits the operating temperature of the apparatus at this time to 2600 K even though the tungsten mesh heater and other components of the experiment chamber can stand higher temperatures (at least 3000 K).

3.2. Sources of Noise

Noise involved in laser-pulse thermal diffusivity measurements are attributed to four origins: electrical, mechanical, electromagnetical, and optical.

Initially, the electronics were troubled by line noise (60-Hz noise) of about 50-μV peak to peak (p-p) without amplification. This noise was eliminated by using batteries as the power source. At present, the main electrical noise is only 2 μV p-p at 200 Hz, at the input level before the amplifier.

Mechanical noise is induced by vibration from the mechanical pump and the laser cooler. Mechanical vibration changes the optical alignment and modulates the intensity of the radiation arriving at the detector. Since this noise is proportional to the total radiation intensity, the relative amplitude of this noise to the signal is independent of the measurement temperature. Measures to limit transmission of mechanical vibration reduced the noise amplitude (resonant frequency is about 50 Hz) from 10% to less than 0.1% of the maximum temperature rise, T_{max}.

Electromagnetically induced noise is due to the AC current through the heater and transient current during the laser charge and discharge. This noise is virtually eliminated by keeping the electronics away from the noise sources.

A small amount of stray light from the laser impinges on the detector through multiple reflections. This produces a very short spike and is separated from the signal on the time scale.

After all the measures against noise are taken, only the mechanical noise is observed at temperatures higher than 1700 K, and the total noise is reduced to a level of less than 0.1% of T_{max}. When the measurement temperature is lower than 1700 K, the electronic noise is largest and is about 1% of T_{max} at 1500 K.

3.3. Maximum Temperature Rise of the Back Surface of the Specimen Due to the Laser Pulse

After the laser energy is absorbed by the specimen, the temperature of the specimen is higher than the steady-state temperature. The maximum temperature rise of the back surface of the specimen, T_{max}, was estimated

from the output voltage of the silicon photodiode, which detects the radiation from the back surface of the specimen. The output voltage was compared with the automatic optical pyrometer at three temperatures under steady-state conditions. In the case of a graphite specimen (POCO AXM-5Q1) of 2-mm thickness and 6.3-mm diameter, T_{max} is about 7 K for a laser energy of about 42 J.

3.4. Characteristics of the Laser Beam

3.4.1. Time History of the Laser Beam Intensity

Figure 4 shows the time history of the intensity of the Nd–glass laser beam measured with the silicon photodiode after attenuation. This shape is reproducible from pulse to pulse. The width at half-maximum signal is 550 μs and cannot be neglected compared to the characteristic time of thermal diffusivity measurements (10–100 ms). Consequently, a correction for finite pulse time is necessary and is discussed in Sections 3.6 and 4.5.

3.4.2. Spatial Profile of the Laser Beam

Figure 5 shows the examples of laser beam profiles obtained with laser footprint paper. The laser was carefully aligned with the help of an autocollimator before obtaining profiles. The total pulse energy was 67 J. Figure 5a shows the result corresponding to exposure to the direct beam.

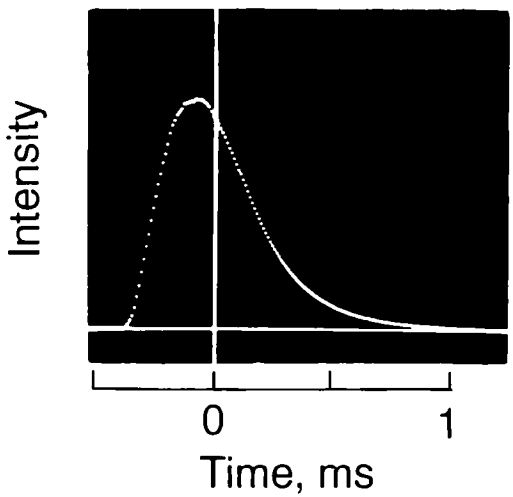

Fig. 4. Time dependence of the intensity of the Nd–glass laser beam. The vertical line indicates the center of gravity of the energy distribution.

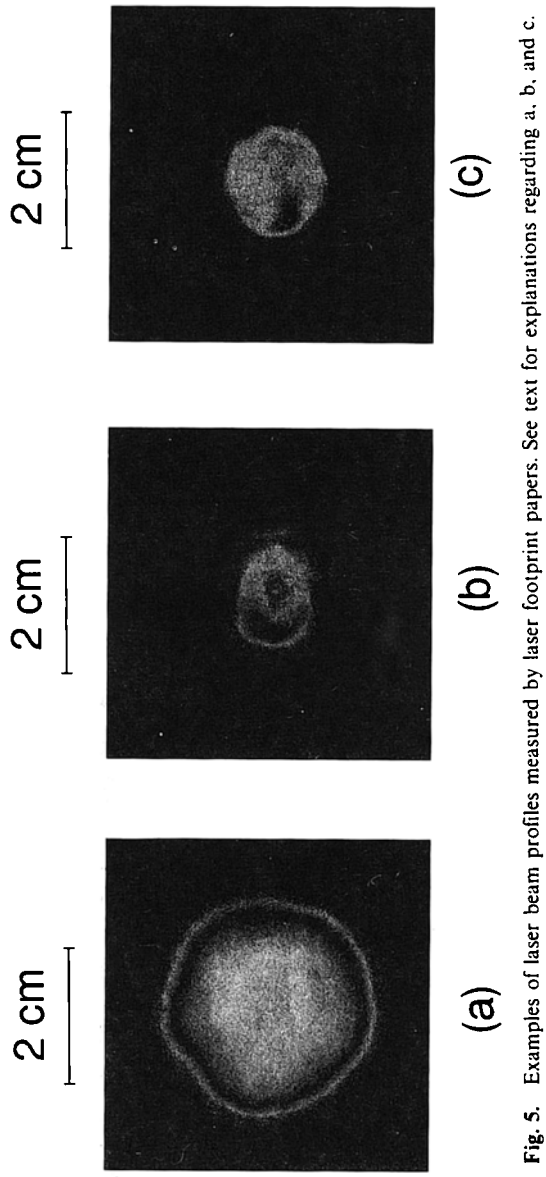

Fig. 5. Examples of laser beam profiles measured by laser footprint papers. See text for explanations regarding a, b, and c.

The distance from the laser head to the footprint paper is set equal to that from the laser head to the specimen. Figures 5b and c show the results corresponding to the exposure to the attenuated beam by reflection from a prism surface, where the distance from the laser head to the footprint paper is kept the same as that in Fig. 5a. The total pulse energy is 67 J for beam b and 71 J for beam c. The attenuation ratio is estimated to be about 10% from the reflectivity of glass at 1.06 μm. The footprint patterns corresponding to b and c without attenuation are both identical to a. These patterns are reproducible from pulse to pulse under the same laser alignment, the same discharge interval, and the same charging voltage. These results demonstrate that even if a footprint paper pattern of a laser beam looks uniform, the uniformity might be due to saturation by an intense beam. Generally, even after careful alignment, the beam profile is irregular as shown in Figs. 5b and c.

3.5. Measurement Procedure

The procedure for a series of thermal diffusivity measurements is as follows. The specimen to be measured is mounted in the specimen holder as shown in Fig. 3. After the specimen holder is placed in the experiment chamber, optical alignment is performed. First, the beam from a He–Ne laser is collimated with the Nd–glass laser beam. Then the prism over the chamber is adjusted so that the He–Ne laser beam illuminates the center of the front surface of the specimen. Adjustment of the detection optics is made by introducing a guide beam from an illumination lamp into the optical fiber bundle from the detector side. The flat mirror under the chamber is adjusted so that the guide beam illuminates the center of the back surface of the specimen.

The heater of the furnace can be turned on after the vacuum level in the chamber is lower than 0.02 Pa. Before making a series of measurements, a trial measurement is made at about 1800 K. The data obtained during the trial measurement are immediately transferred from the digital oscilloscope to the computer and are analyzed. If the specimen is pulse heated by the nonuniform part of the laser beam, the experimental curve cannot be fitted satisfactorily by the theoretical curve. At this point, the measurement is stopped and a new trial measurement is made, either making use of another part of the laser beam or after realigning the laser to improve the beam profile.

If the experimental curve is fitted closely by the theoretical curve, the main measurements are started. Usually an experiment is performed every 100 K. It takes about 20 min for the furnace to establish temperature equilibrium after the heater current is changed.

The system is operated from outside the experiment room to avoid exposure to the laser beam. After the laser is activated remotely, data are automatically recorded by the digital oscilloscope. The output voltage of the automatic pyrometer is recorded immediately before and after the laser discharge. The data are transferred from the digital oscilloscope to the computer and are processed.

3.6. Data Analysis

3.6.1. Basic Equation

The analytical solution for laser-pulse thermal diffusivity measurements has been given by Parker et al. [1] under the following conditions:

(1) The duration of the laser pulse is negligibly short compared to the characteristic time of thermal diffusion.

(2) The front surface of the specimen is uniformly heated by a spatially homogenized laser beam.

(3) The specimen is adiabatic during the measurement after the laser energy is absorbed.

(4) The specimen is uniform (in geometry) and is homogeneous.

(5) The specimen is nontransparent to the laser beam and to thermal radiation.

If these conditions are satisfied, the heat flow becomes one-dimensional and the temperature of the back surface of the specimen changes according to the following equation:

$$T(t) = T_M \left[1 + 2 \sum_{n=1}^{\infty} (-1)^n \exp\left(-n^2 \frac{t}{t_0} \right) \right] \tag{1}$$

where $T_M = Q/C$, the maximum temperature rise of the rear surface of the specimen with no heat loss; Q is the total energy absorbed by the specimen; C, the heat capacity of the specimen, and $t_0 = l^2/(\pi^2 \alpha)$, the characteristic time of thermal diffusion; l, the thickness of the specimen; and α, the thermal diffusivity of the specimen.

Because the radiative heat loss from the specimen is unavoidable for measurements above 1500 K, assumption (3) is not valid and Eq. (1) cannot be used to analyze the data obtained with the present apparatus. Cape and Lehman [7] gave a general solution for the laser-pulse thermal diffusivity measurements which took the radiative heat loss and the finite pulse time effects into consideration. The original formula of their general solution is given in their paper.

The contribution of the radiative heat loss is expressed by nondimensional parameters called Biot numbers. The Biot number is defined as $Y_x = 4\varepsilon_s \sigma T_0^3 l/\lambda$ for the front and the back surface of the specimen since the radiative heat loss in this direction does not return to the specimen again. If the configuration between the specimen and the holder is considered, there is only a small gap between the cylindrical side of the specimen and the inside wall of the holder. Thus, the radiative heat loss from the side surface of the specimen is smaller than heat losses from the front surface and the back surface of the specimen. The lower limit is the value when all emitted radiation is reflected back to the side surface of the specimen with the reflectance of tungsten. In this case the Biot number is expressed as $Y_r = [4\sigma T_0^3 r_0/\lambda]\, \varepsilon_s \varepsilon_h / [1 - (1 - \varepsilon_s)(1 - \varepsilon_h)]$ for the radiative heat loss from the cylindrical side surface of the specimen where ε_s and ε_h are the total hemispherical emissivity of the specimen and the specimen holder, respectively, r_0 is the radius of the specimen, T_0 is the steady-state temperature of the specimen, λ is the thermal conductivity of the specimen, and σ is the Stefan–Boltzmann constant.

When Y_x and Y_r are considerably less than 1, Cape and Lehman presented an approximate formula for their general solution:

$$T(t) = T_M \sum_{m=0}^{\infty} A_m \exp\left[-M_m \frac{t}{t_0} \right] \tag{2}$$

where

$$A_m = 2(-1)^m X_m^2 (X_m^2 + 2Y_x + Y_x^2)^{-1}$$

$$M_m = [X_m^2 + (l/r_0)^2 z_0^2]/\pi^2$$

$$z_0 = (2Y_r)^{1/2} (1 - Y_r/8)$$

$$X_0 = (2Y_x)^{1/2} (1 - Y_x/12 + 7Y_x^2/288)$$

for $m \geqslant 1$

$$X_m = m\pi + 2Y_x/m\pi - 4Y_x^2/(m\pi)^2 - 2Y_x^3/3(m\pi)^3 + 16Y_x^4/(m\pi)^4$$

For example, the Biot number Y_x is 0.20 when a graphite specimen of 2.4-mm thickness is measured at 2500 K. The error due to truncating the fourth-order term in the series is less than 0.1%. The ratio of $7Y_x^2/288$ to 1 is 0.1% and the ratio of $16Y_x^4/(m\pi)^4$ to $m\pi$ is less than 0.01%.

3.6.2. Conventional Analysis Methods in the Literature

When the five conditions in Section 3.6.1 are satisfied, the thermal diffusivity is calculated from the measured time–temperature curve based on the "$t_{1/2}$ method" [1]. The half-rise time, $t_{1/2}$, is defined by the interval required for the back-surface temperature to reach one-half of the

maximum temperature rise. The thermal diffusivity is calculated as $\alpha = 1.370l^2/(\pi^2 t_{1/2})$, where l is the thickness of the specimen. Since the $t_{1/2}$ method is not valid if any of the five conditions is not satisfied, it cannot be applied to high-temperature measurements above 1500 K, where radiative heat loss is unavoidable.

There are a few algorithms to calculate thermal diffusivity from the data obtained by the laser-pulse methods which take the radiative heat loss into consideration. Among them, Cowan's [8] and Clark and Taylor's [9] methods are most commonly used. Their methods are in contrast with each other because the former uses the cooling part of the curve, whereas the latter uses the heating part of the curve to correct for the radiative heat loss. Takahashi et al. [10] proposed a correction method similar to Cowan's method. Their method calculates the correction factor for radiative heat loss from the ratio of $t_{1/2}$ to τ, which is the characteristic time of the radiative cooling.

To apply Cowan's method or Takahashi's method successfully, drift of the steady-state temperature and conduction heat loss must be small. On the other hand, Clark and Taylor's method requires a high signal-to-noise ratio.

3.6.3. A New Method of Data Analysis

Contrary to the conventional data analysis methods, the new method introduced in this paper uses the entire temperature rise curve after the laser energy was absorbed by the specimen. The entire curve including both heating and cooling parts is best fitted by the theoretical curve expressed by Eq. (2), which is called "a curve-fitting method". The ratio of Y_x and Y_r is given based on $Y_r = \varepsilon_h/[1-(1-\varepsilon_s)(1-\varepsilon_h)](r_0/l)\, Y_x$, substituting literature values of ε_s and ε_h and dimensions l and r_0.

Two types of data analysis programs are used. The first type neglects the radiative heat loss in the radial direction ($Y_r = 0$ and $Y_x = Y$). Equation (2) is simplified in this approximation to yield the following equation:

$$T(t) = T_M \sum_{m=0}^{\infty} A_m \exp\left[-\left(\frac{X_m}{\pi}\right)^2 \frac{t}{t_0}\right] \tag{3}$$

where

$$A_m = 2(-1)^m X_m^2 (X_m^2 + 2Y + Y^2)^{-1}$$

$$X_0 = (2Y)^{1/2}\,(1 - Y/12 + 7Y^2/288)$$

$$\text{for } m \geqslant 1$$

$$X_m = m\pi + 2Y/m\pi - 4Y^2/(m\pi)^2 - 2Y^3/3(m\pi)^3 + 16Y^4/(m\pi)^4$$

The second type of program takes into account the radiative heat loss in the radial direction as well as in the axial direction in Eq. (2). As described in Section 4.7, the difference in the calculated thermal diffusivity value from the first program and the second program is less than 5% of the magnitude of the radiative heat loss correction. Hence, the first program is regularly used for analysis of measured temperature history curves.

An example of the data analysis procedure to determine thermal diffusivity values by the curve-fitting method is shown in Fig. 6. The experimental data were obtained for a graphite specimen of 2-mm nominal thickness at 1694 K. First, the time origin is set at the center of gravity of energy distribution of the laser pulse as shown in Fig. 4. The analysis assumes that the surface of the specimen is uniformly heated by the delta function pulse at this time. According to Eq. (3), when t is much larger

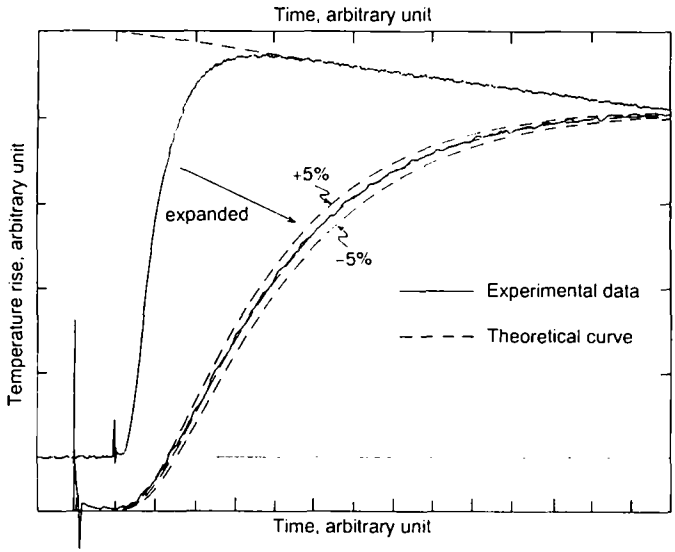

Fig. 6. Procedure of data analysis by the curve-fitting method. First, the cooling part ($t > 8t_0$) of the experimental data is least-squares fitted to the exponential curve, $T(t) = T_M A_0 \exp(-t/\tau)$, and τ is fixed. Then the characteristic time, t_0, is expressed by a single valued function of the Biot number, Y, as $t_0 = \tau\, 2Y(1 - Y/12 + 7Y^2/288)^2/\pi^2$. The value of Y is determined to minimize the deviation between the experimental data (solid curve) and Cape and Lehman's theoretical equation (dashed curves). Thus, Y and t_0 are fixed and the thermal diffusivity is obtained as $\alpha = l^2/(\pi^2 t_0)$. When a thermal diffusivity value 5% larger or smaller than the best fitted value is substituted in the theoretical equation, the theoretical curve deviates considerably from the experimental data.

than t_0, the first term becomes dominant over the other terms. Consequently, the temperature rise decreases exponentially with the characteristic cooling time of $\tau = t_0/(X_0/\pi)^2$. After τ is determined by a least-squares fit, t_0 is a single-valued function of Y. This means that Y is the only parameter that varies. When the best fit to the heating part of the curve is obtained, t_0 is uniquely determined and thermal diffusivity is calculated as $\alpha = l^2/(\pi^2 t_0)$.

Figure 7 shows another example of the experimental data on graphite at 2248 K and the fitted theoretical curve. Since the signal-to-noise ratio is improved at temperatures higher than 2000 K, it is very difficult to distinguish the theoretical curve from the experimental data in the figure. The origin of the time scale is intentionally shifted between the experimental data and the theoretical curve in Fig. 7 for display purposes.

The curve-fitting method is a comprehensive method in the sense that most of the conventional methods are included as parts of it. For example, when it is applied to the experimental data with no heat loss and only a small segment around the $t_{1/2}$ point is chosen for the fitting procedure, it is essentially the same as the $t_{1/2}$ method. This fact is demonstrated by com-

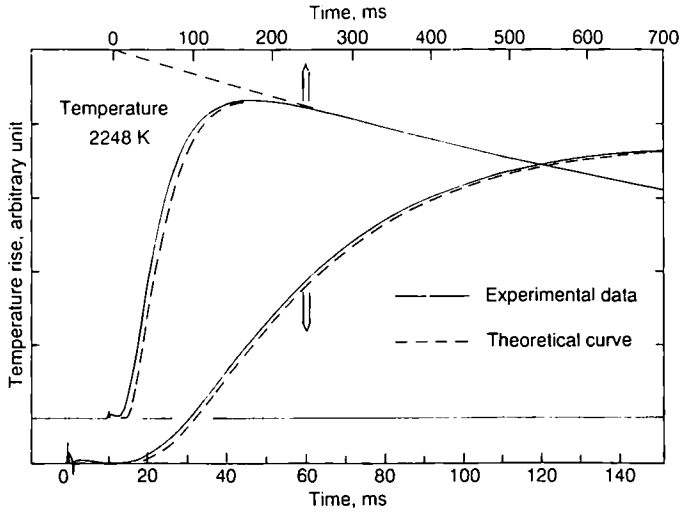

Fig. 7. Example of real transient temperature history curves for a graphite specimen of 6.3-mm diameter and 1.981-mm thickness analyzed by the curve-fitting method. The origin of the time scale is intentionally shifted between the experimental data (solid curve) and the theoretical curve (dashed curve) for display purposes. The calculated thermal diffusivity is 0.0944 $cm^2 \cdot s^{-1}$ and the Biot number is 0.146.

parison of calculated thermal diffusivity values based on "different" data analysis algorithms from the "same" temperature history curve. Table I lists thermal diffusivity calculated by the present curve-fitting method compared with those calculated by various conventional methods of data analysis from the experimental data shown in Fig. 1 of Ref. 11 and another set of data of quality similar to those shown in Fig. 7. There is essentially no difference between the thermal diffusivity values obtained by the data analysis methods after heat loss correction. This result is quite reasonable because all methods tried are based on the same theoretical formula, and consequently, if the experimental data are obtained under the same conditions as assumed by the theoretical calculation, all methods should give the same thermal diffusivity value.

The special advantage of the curve-fitting method over the other methods is that the quality of experimental data can be checked by observing the discrepancy between the experimental data and the theoretical curve. Data of poor quality such as those affected by nonuniform heating, by drift of steady-state temperature, or by a temperature detection system of slow response time can be excluded immediately. Thus, only experimental data of good quality are chosen and thermal diffusivity values with a smaller uncertainty are obtained.

Table I. Comparison Between Calculated Thermal Diffusivity Values Based on Different Data Analysis Algorithms from the Same Temperature History Curve

Temperature history curve	Fig. 1 in Ref. 11	Not shown
Specimen temperature (K)	1696	2248
	Thermal diffusivity ($cm^2 \cdot s^{-1}$)	
Curve-fitting (present) method	0.1137	0.0950
Cowan [8]		
$T(5t_{1/2})/T(t_{1/2})$	0.114	0.095
$T(10t_{1/2})/T(t_{1/2})$	0.114	0.095
Clark and Taylor [9]		
$t_{0.7}/t_{0.3}$	0.114	0.095
$t_{0.8}/t_{0.4}$	0.114	0.095
$t_{0.8}/t_{0.2}$	0.115	0.095
Takahashi et al. [10], $t_{1/2}/\tau$	0.114	0.094
$t_{1/2}$ method (without heat loss correction)	0.119	0.104

4. ESTIMATE OF ERRORS

4.1. Specimen Temperature

4.1.1. Calibration of the Automatic Pyrometer and the Window

The automatic pyrometer is calibrated against a NIST-calibrated gas-filled tungsten-filament reference lamp. Uncertainty in the lamp calibration against the temperature scale is ± 1 K at 1800 K and increases to ± 2 K at 2500 K.

The pyrometer is calibrated with the quartz window plate placed in the optical path between the pyrometer and the reference lamp. During use, transmission of the window decreases due to contamination with materials vaporized from the hot components in the experiment chamber. This change corresponds to <2 K at 2500 K after operation of the apparatus for several tens of hours.

4.1.2. Blackbody Quality

Thermal radiation from the specimen holder is observed through the side hole (2.4 mm in diameter). The quality of the specimen holder as a blackbody cavity is estimated experimentally. Assuming that the temperature of the specimen holder is uniform, the effective emissivity of the cavity is equal to the effective absorptance of the cavity according to Kirchhoff's law. Therefore, the effective emissivity can be obtained by measuring the effective absorptance of a beam which illuminates the side hole of the specimen holder at room temperature. A He–Ne laser is used as an illumination source for this purpose because the wavelength of the He–Ne laser (633 nm) is close to the pyrometer wavelength (650 nm).

The absorptance of the cavity is determined by measuring the ratio of the reemitted light which is not absorbed in the cavity to the intensity of the illuminating beam. Most of the reemitted light comes from the aperture of the diaphragm on the top of the specimen holder as shown in Fig. 3. The intensity of the reemitted light is measured with the optical fiber bundle and the silicon photodiode. The intensity is integrated over the aperture area and divided by the total intensity of the input laser beam. This ratio is 0.002 and thus the effective emissivity of the specimen holder observed from the side hole is estimated to be 0.998. The cavity with the effective emissivity of 0.998 yields a radiance temperature 0.6 K lower than the inside wall temperature at 2500 K.

4.1.3. Temperature Difference Between the Specimen and the Cavity

Heat conduction between the specimen and the specimen holder is negligibly small because they make only pinpoint contact with each other. Since the specimen is surrounded by the specimen holder and does not see the heater element directly, the specimen temperature is determined by the balance of radiative heat transfer among the specimen, the specimen holder, and the room temperature environment.

As shown in Fig. 3, the front surface of the specimen sees the inside of the specimen holder and the quartz plate of the top window at room temperature. The solid angle of the aperture seen from the specimen, Ω_f, is 0.17. The back surface of the specimen sees the inside of the tungsten tube and the quartz plate of the bottom window which is at room temperature. The solid angle of the other end opening of the tungsten tube seen from the specimen, Ω_r, is 0.04. The cylindrical side of the specimen sees only the inside of the tungsten specimen holder because of the close fit. The radiative heat transfer between them can be treated as if they are two infinite wall surfaces facing each other.

The equation of the energy balance by radiative heat transfer is formulated assuming that the temperatures of the specimen holder and the tungsten tube are uniform and the same, T_h. When the temperature of the specimen is T_s and room temperature radiation is neglected, the energy balance of the specimen by radiative heat transfer is expressed by the following equation:

$$\begin{aligned}(A_f + A_b)\,\varepsilon_s \sigma T_s^4 + A_s \frac{\varepsilon_h \varepsilon_s}{1-(1-\varepsilon_h)(1-\varepsilon_s)} \sigma T_s^4 \\ = A_f\left(1-\frac{\Omega_f}{\pi}\right)\varepsilon_s \sigma T_h^4 + A_b\left(1-\frac{\Omega_r}{\pi}\right)\varepsilon_s \sigma T_h^4 \\ + A_s \frac{\varepsilon_h \varepsilon_s}{1-(1-\varepsilon_h)(1-\varepsilon_s)} \sigma T_h^4 \end{aligned} \tag{4}$$

Solving for T_s,

$$T_s = T_h \sqrt[4]{\frac{\left[\left(1-\frac{\Omega_f}{\pi}\right)A_f + \left(1-\frac{\Omega_r}{\pi}\right)A_b + \frac{\varepsilon_h}{1-(1-\varepsilon_h)(1-\varepsilon_s)} A_s\right]}{\left[A_f + A_b + \frac{\varepsilon_h}{1-(1-\varepsilon_h)(1-\varepsilon_s)} A_s\right]}} \tag{5}$$

where A_f, A_b, and A_s are the areas of the front, back, and cylindrical side surface of the specimen, respectively; ε_s is the total hemispherical emissivity of the specimen; and ε_h is that of the specimen holder.

If a graphite specimen of 2-mm thickness and 6.3-mm diameter is used, ε_s is approximately 0.8, A_f is 31.2 mm^2, A_b is 31.2 mm^2, and A_s is 39.6 mm^2. The total hemispherical emissivity of tungsten, ε_h, at 2000 K is 0.32 [12]. Substituting these values in Eq. (5), we obtain $T_s = 0.993\ T_h$. This equation is also valid if the thickness of the specimen is 1.5 or 2.5 mm [$T_s = (0.993 \pm 0.0005)\ T_h$]. The absolute temperature of the specimen is estimated to be 99.3% of that of the specimen holder.

It should be noted that the effective temperature of the specimen attributed to the thermal diffusivity measurement is higher than the steady-state temperature because of the pulse heating. It is assumed that 1.6 times the transient maximum temperature rise T_{max} is added to the steady-state temperature based on the calculation by Parker et al. [1]. The uncertainty in the effective temperature of the specimen related to this correction is estimated to be less than half of T_{max}.

The uncertainty in the thermal diffusivity resulting from the difference in the effective temperature rise is experimentally evaluated by measuring the thermal diffusivity with varying laser power as shown in Fig. 8. When the transient maximum temperature rise T_{max} of the graphite specimen of 1.981-mm thickness changes from about 4 to 9 K at the steady-state temperature of 1887 K, the standard deviation in the measured thermal diffusivity values is 0.32%. Since this is close to the standard deviation of thermal diffusivity values measured under constant laser power as shown in Fig. 9, it can be said that the uncertainty in the thermal diffusivity resulting

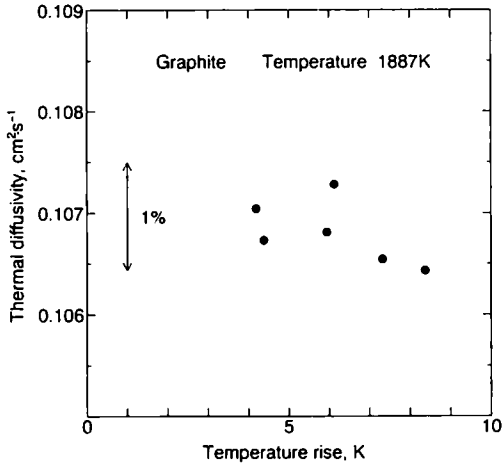

Fig. 8. Scattering of measured thermal diffusivity values of graphite with different transient temperature rises (at 1887 K).

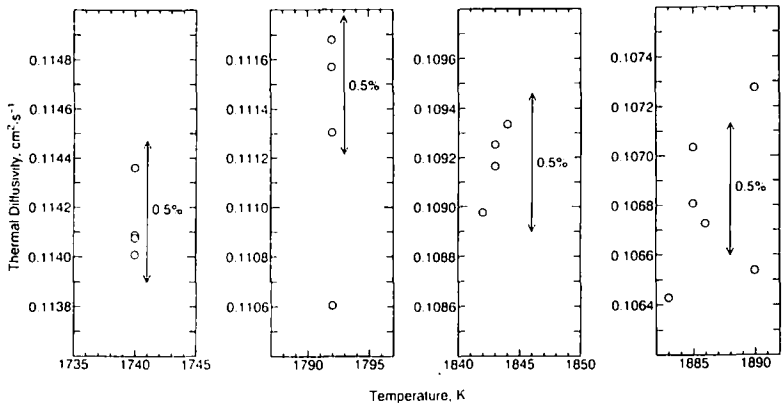

Fig. 9. Scattering of the calculated thermal diffusivity values of graphite due to both the short-term reproducibility of the measurements and the imprecision of the curve fitting.

from the difference in the effective temperature rise is smaller than 0.3%. It should be also noted that the difference in the thermal diffusivity of graphite at 1500 and at 1510 K is only 0.5% [11].

4.2. Specimen Thickness

Thermal diffusivity is related to the square of the specimen thickness. Thus $\Delta\alpha/\alpha = 2\Delta l/l$, and when a specimen of 2-mm thickness is used, both surfaces of the specimen must be polished parallel within 10 μm ($\pm 0.25\%$ in thickness) to reduce the uncertainty in thermal diffusivity due to the specimen thickness to less than 0.5%.

4.3. Performance of the Detector Optics and the Electronics

The total response time of the detector optics and the electronics is determined to be less than 10 μs. Since the signal response of the silicon photodiode is linear to the input radiation for small temperature changes (of the order of 10 K), the total nonlinearity is attributed mainly to the nonlinear dependence of the Planck's formula on temperature. The maximum transient temperature rise, T_{max}, at the back surface is usually less than 10 K at temperatures of 1500–2500 K. Planck's formula can be approximated by a linear function with a discrepancy less than 1% within this small temperature change. The validity of this linear approximation is indirectly supported by the agreement between the experimental curve and the theoretical curve as shown in Figs. 6 and 7.

4.4. Performance of the Digital Data Acquisition System

The operational characteristics of the digital oscilloscope used are as follows.

Signal resolution:	12 bits (0.025%).
Maximum sweep length:	4096 points.
Time base accuracy:	0.01%.
Overall accuracy:	0.2% (full scale).
Linearity:	0.1% (full scale).

Of these characteristics, time base accuracy and linearity are especially important for obtaining accurate thermal diffusivity values. The uncertainties in both of these quantities are negligibly small compared to the other error sources.

4.5. Uncertainty of the Time Origin

The digital oscilloscope is triggered by the laser radiation pulse, which is picked up from the mirror of the laser cavity by an optical fiber bundle and detected by a silicon photodiode. Since the signal rises fast, the time of triggering is reproducible with much better precision than the sampling period of the digital oscilloscope (100 μs).

In our analysis, the real laser pulse is approximated by a delta function at the center of gravity of the pulse, i.e., at the time at which the moment of energy distribution of the pulse balances. The time dependence of the laser beam intensity shown in Fig. 4 was taken using the same trigger. Calculations showed that the center of gravity of the pulse is located 600 μs after the trigger time. Consequently, if data processing is done assuming that the origin of the time base is 600 μs after the trigger time, the uncertainty of the origin of the time is less than 100 μs. When measurements on a graphite specimen of 1.5-mm thickness are made, the characteristic time of thermal diffusion is about 20 ms. So an uncertainty of 100 μs in the origin of the time corresponds to an uncertainty of 0.5% in the thermal diffusivity value. The uncertainty associated with approximating the center of gravity of the pulse at the origin of the time base is estimated to be much smaller than 0.5% [13].

4.6. Nonuniform Heating effect

A typical example of the laser beam profile of the Nd–glass laser is shown in Figs. 5b and c. It was difficult to obtain a more uniform laser beam than shown in Figs. 5b and c even after careful alignment of the laser

cavity. Therefore, errors due to nonuniform heating cannot be neglected in our measurements [14].

Figure 10 shows the thermal diffusivity values of the same graphite specimen at the same temperature obtained by choosing different portions of the laser beam. The horizontal axis indicates the average deviation between the experimental curve and the fitted theoretical curve. During this set of measurements, only the energy distribution of the beam which impinged on the surface of the specimen was changed; the other experimental conditions were kept the same. The results show that there is an error due to nonuniform heating which may be as large as 8% p-p if an arbitrary portion of the laser beam is randomly chosen to impinge on the surface of the specimen.

To reduce the error due to nonuniform heating, the beam uniformity was judged by the fit of the theoretical curve to the experimental $t - \Delta T$ curve, as discussed in Section 3.5. The scattering of thermal diffusivity values converges when the average deviation becomes small. After introducing this criterion, the deviation of thermal diffusivity values was reduced to a value as small as 2% p-p.

4.7. Radiative Heat Loss Effects

Conduction heat loss is expected to be negligibly small because the specimen is supported by tiny projections. However, radiative heat loss is

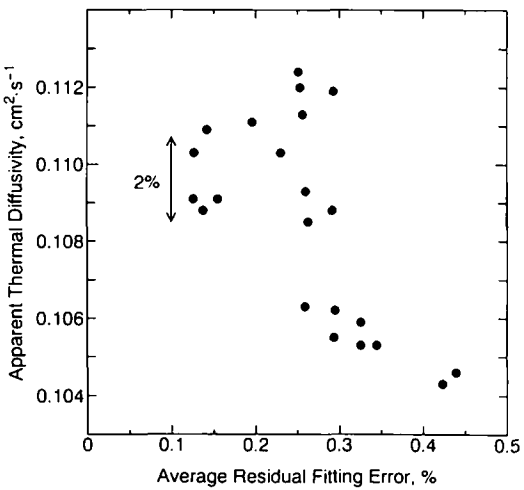

Fig. 10. Scattering of apparent thermal diffusivity values of graphite due to the irregularity of the incident laser beam (at 1797 K).

unavoidable for the measurements at temperatures above 1500 K. Since the adiabatic assumption for the specimen is invalid, our new data analysis method stated in Section 3.6 takes the radiative heat loss into consideration from the beginning. As described in Section 3.6, analytical calculation can be made with an accuracy better than 0.1% using a computer. Thus the major ambiguity is related to the anisotropy of the radiative heat loss since it is very difficult to determine the ratio of Y_r to Y_x experimentally.

If the literature values of 0.32 for the emissivity of tungsten [12] and 0.8 for graphite [15] are used, Y_r is $0.37(r_0/l)\,Y_x$ as described in Section 3.6, where Y_r is the Biot number in the radial direction and Y_x is the Biot number in the axial direction. Thus, two values of thermal diffusivity have been obtained from the same experimental $t-\Delta T$ curve with two types of programs, the first type with $Y_r=0$ and the second type with $Y_r=0.37(r_0/l)\,Y_x$. The difference between the two calculated thermal diffusivity values is less than 5% of the magnitude of the radiative heat loss correction.

4.8. Uncertainty Associated with Data Analysis and Short-Term Reproducibility

The uncertainty associated with data analysis is closely related to the uncertainty of the time origin (Section 4.5), the nonuniform heating effect (Section 4.6), and the radiative heat loss effects (Section 4.7). Since these errors have already been estimated, the precision and reproducibility of the curve fitting is discussed in this section. During the fitting procedure, the average deviation of the theoretical curve from the experimental curve is calculated. The iterative calculation is stopped after the residual average deviation decreases to a value less than 0.01% of the maximum temperature rise. The precision of the curve fitting is indirectly estimated from the scattering of the thermal diffusivity values of graphite obtained from the successive measurements over a period of one hour as shown in Fig. 9. The standard deviation of the scattering, which includes the precision of the curve fitting method, is less than 0.5%.

4.9. Summary of Error Analysis

Based on the analysis of the sources of errors likely to affect the determination of thermal diffusivity with the present system, it can be said that thermal diffusivity can be determined with an uncertainty not exceeding 3% in the temperature range 1500 to 2500 K. The specific value of the uncertainty depends, to some extent, on the material and the condition of the specimen, as well as on the temperature.

A detailed discussion of the sources and magnitudes of the errors in connection with extensive measurements on graphite in the range 1500 to 2500 K with the present apparatus is given in another paper [11].

5. CONCLUSION

Temperature history signals with an excellent signal-to-noise ratio, a fast response time, and sufficient linearity were obtained with this high-temperature laser-pulse thermal diffusivity apparatus in the range 1500 to 2500 K. Introduction of the new data analysis method solved the problem of the radiative heat loss from the specimen and reduced the error due to nonuniform heating. The uncertainty in thermal diffusivity values is estimated to be not more than 3% at 2500 K. The uncertainty in specimen temperature is estimated to be not more than 10 K at 2500 K. This apparatus with the new data analysis method has been used successfully to measure the thermal diffusivity of POCO AXM-5Q1 graphite from 1500 to 2500 K [11].

It is noted that the nonuniform heating of the front surface of the specimen remains the single major problem which needs to be solved to reduce the uncertainty of thermal diffusivity measurements further. A technique to homogenize the laser beam profile is essential for this purpose [14, 16].

ACKNOWLEDGMENTS

Two of the authors (T.B. and R.T.) acknowledge the support of their respective organizations and the National Institute of Standards and Technology (NIST) during their stay at NIST as guest scientists. The authors would like to express their sincere appreciation to A. P. Miiller and J. L. McClure for their help in various phases of this work.

REFERENCES

1. W. J. Parker, R. J. Jenkins, C. P. Butler, and G. L. Abbott, *J. Appl. Phys.* **32**:1679 (1961).
2. R. E. Taylor and K. D. Maglić, in *Compendium of Thermophysical Property Measurement Methods, Vol. 1. Survey of Measurement Techniques*, K. D. Maglić, A. Cezairliyan, and V. E. Peletsky, eds. (Plenum, New York, 1984), p. 305.
3. F. Righini and A. Cezairliyan, *High Temp.-High Press.* **5**:481 (1973).
4. R. Taylor, *J. Phys. E Sci. Instrum.* **13**:1193 (1980).
5. R. U. Acton and J. A. Kahn, Paper presented at the 10th Thermal Conductivity Conference, Boston, MA (1970).
6. R. E. Taylor, *High Temp.-High Press.* **11**:43 (1979).
7. J. A. Cape and G. W. Lehman, *J. Appl. Phys.* **34**:1909 (1963).

8. R. D. Cowan, *J. Appl. Phys.* **14**:926 (1963).
9. L. M. Clark III and R. E. Taylor, *J. Appl. Phys.* **46**:714 (1975).
10. Y. Takahashi, T. Azumi, and M. Sugano, *Netsu Sokutei* **8**:62 (1981) (in Japanese).
11. T. Baba and A. Cezairliyan, *Int. J. Thermophys.* **15**:343 (1994).
12. A. Cezairliyan and J. L. McClure, *J. Res. Natl. Bur. Stand. (U.S.)* **75A**:283 (1971).
13. T. Azumi and Y. Takahashi, *Rev. Sci. Instrum.* **52**:1411 (1981).
14. T. Baba, M. Kobayashi, A. Ono, J. H. Hong, and M. M. Suliyanti, *Thermochim. Acta* **218**:329 (1993).
15. A. Cezairliyan and F. Righini, *Rev. Int. Hautes Temp. Refract.* **12**:124 (1975).
16. T. Baba, J. H. Hong, and A. Ono, in *Proceedings of the 2nd Asian Thermophysical Properties Conference*, Sapporo, Japan (1989), p. 127.